Journal of Solid State Electrochemistry (2018) 22:2821–2828
https://doi.org/10.1007/s10008-018-3990-3

ORIGINAL PAPER

Electrochemical behavior of $CoSb_3$ in sulfuric and oxalic acids over the potential range 0 to 40 V

Delphine Veys-Renaux[1] · Richard Drevet[1] · Carine Petitjean[1] · Lionel Aranda[1] · Nicolas David[1] · Patrice Berthod[1]

Received: 21 November 2017 / Revised: 15 April 2018 / Accepted: 4 May 2018 / Published online: 23 May 2018

Abstract

The electrochemical behavior of pure Co, pure Sb, and $CoSb_3$ has been investigated over a large anodic potential range (0 to 40 V) in two acids, i.e., oxalic acid or sulfuric acid at different concentrations (0.01 to 1 M). Potentiodynamic polarizations performed on $CoSb_3$ plates reveal the possible formation of a passive layer between 1 and 3 V (vs SCE), on a passivation plateau. The oxidation of $CoSb_3$ at 2 V in sulfuric and oxalic acids results in the growth of an anodic conversion layer. This coating is mainly made of a porous layer of amorphous antimony oxides due to dealloying of $CoSb_3$. In the specific case of oxalic acid, rods of crystallized oxalates are tangled between the oxide sheets.

Keywords Intermetallics · Thin films · Anodization · Dealloying · SEM

Introduction

$CoSb_3$-based skutterudite compounds are promising thermoelectric materials thanks to a high figure of merit ZT [1]. However, their sensitivity to thermal degradation under oxidation mechanisms is a significant problem regarding their use at high temperature [2–5]. Actually, the exposition of $CoSb_3$ to air at operating temperatures (until 800 K) results in the formation of a non-protective scale layer. The oxidation mechanism consists in a selective outward diffusion of antimony and inward diffusion of oxygen. Consequently, the inner oxide layer is mainly made of a mixed oxide $CoSb_2O_4$, and the outer layer is made of a mixture of volatile antimony oxides Sb_2O_3 and Sb_2O_4. Depending on the temperature, an intermediate layer of $CoSb_2O_6$ may also be formed.

The high rate of degradation of $CoSb_3$, induced by the high mobility of antimony through the oxide layer and the volatility of antimony oxides (especially Sb_2O_3), limits the thermoelectric devices durability.

A protective coating is therefore necessary to prevent the oxidation reactions. At the same time, the thermoelectric properties must be maintained. Therefore, a coating with oxides seems to be the most judicious solution. Among the few papers dealing with the formation of coatings, most of them relate the use of physical vapor deposition [6–11]. A very recent one describes the deposition of a glass coating by a dipping technique [12].

In this framework, the formation of an oxide conversion layer by surface anodizing represents an interesting alternative to the methods usually considered. Actually, the anodizing, consisting in the electrochemical oxidation of a sample in an aqueous electrolyte, is a cheap and easy to use way of surface conversion, even on pieces with a complex geometry. The resulting layers are well adherent. To the best of our knowledge, electrochemical anodizing of $CoSb_3$ has never been studied.

Therefore, this work aims at presenting for the first time electrochemical conversion of $CoSb_3$. For that purpose, two acidic media have been chosen as electrolytes: sulfuric acid (H_2SO_4) and oxalic acid (HOOC–COOH) [13–16].

In order to determine the most suitable anodizing conditions, the electrochemical behavior of $CoSb_3$ has been investigated over a wide range of potentials [17–20]. Furthermore, in order to highlight the relative contribution of cobalt and antimony regarding the behavior of the $CoSb_3$ intermetallic phase, the electrochemical study has also been carried out on pure metallic cobalt and pure metallic antimony for comparison. The mechanism of the conversion layers formation has been explained by combining electrochemical results on the

✉ Delphine Veys-Renaux
delphine.veys-renaux@univ-lorraine.fr

[1] Institut Jean Lamour, UMR 7198 CNRS-Université de Lorraine, Campus Artem, allée André Guinier, BP50840, 54011 Nancy cedex, France

one hand and morphological and composition characterizations by scanning electron microscopy and X-ray diffraction on the other hand.

Material and methods

Materials

Pure cobalt plates (99.5%, 3 mm thick) were provided by Goodfellow. Pure antimony plates were prepared by melting pure antimony pieces in an alumina crucible placed in a muffle furnace and casting into an appropriate mold ($10 \times 3 \times 0.3$ cm^3).

$CoSb_3$ alloys were prepared from pure Co (99.99%, Strem Chemicals) and pure Sb (99.999%, Chempur), by melting in a vitreous carbon crucible positioned in a quartz tube under partial Ar pressure. After an optimized thermic cycle, the resulting ingot was reduced into powder and densified under vacuum by spark plasma sintering (SPS) at 630 °C during 10 min under 50 MPa in a commercial system (SPS Syntex 515S). Cylindrical samples (10 mm diameter, 3 mm thick) were finally obtained.

All samples were ground with SiC paper until 1200 grit before electrochemical investigation.

Electrochemical studies

The anodic behaviors of pure Co, pure Sb, and $CoSb_3$ were comparatively investigated in two acidic media, i.e., sulfuric acid (H_2SO_4) and oxalic acid (HOOC–COOH) in concentrations varying between 0.01 and 1 M. Metallic plates (Co, Sb, $CoSb_3$) were mounted as a working electrode at the bottom of a classic "three-electrode cell" (circular active area, 0.5 cm^2), facing to a platinum disk. A Saturated Calomel Electrode (SCE) was used as a reference electrode, and all potentials will be given versus this reference. Potentiodynamic polarizations were performed with a scan rate of 40 mV s^{-1} over the range 0 to 50 V by using the dedicated potentiostat Modulab HV100.

Conversion layers were formed by applying 2 V during 60 min on $CoSb_3$ substrate in sulfuric acid and oxalic acid 0.1 M.

Morphological and structural characterization of the conversion layers

The surface morphology of the grown conversion layers was observed from secondary electron (SE) images obtained with a field emission gun scanning electron microscope (FEG-SEM, HITACHI S-4800). Moreover the cross sections of the samples were observed from backscattered electron (BSE) images after polishing with an argon ion (Ar^+) beam produced by a cross-sectional polisher (JEOL, IB-09010CO). Punctual elemental compositions of the coatings were evaluated semi-quantitatively by energy dispersive spectroscopy (EDS), and EDS maps of O, Sb, and Co were recorded.

The crystalline structure of the anodic layers was assessed by X-ray diffraction (XRD) with a Philips X'pert pro diffractometer using a monochromatic $Cu_{K\alpha}$ radiation ($\lambda = 0.15406$ nm). The patterns were collected from $2\theta = 10°$ to 100° with a step of 0.033°. The structures are identified from the diffraction file provided by the International Centre for Diffraction Data (ICDD).

Results

Electrochemical behavior

The potentiodynamic polarization curves obtained for the Co, Sb, and $CoSb_3$ samples immersed in H_2SO_4 solutions in different concentrations (0.01, 0.1, and 1 M) are displayed in Fig. 1a–c, respectively.

Regarding the anodic polarization of pure Co (Fig. 1a), the values of the current densities highly depend on the electrolyte concentration. As revealed by the linear evolution of the current density over all the potential range, the electrochemical interface obviously behaves as a purely resisting system in the lowest concentrated medium. Regarding the electrochemical behavior in H_2SO_4 0.1 and 1 M, three stages can be distinguished: Actually, in both cases, the linear evolution of the current density is interrupted by a "pseudo passivation plateau," between 1 and 2 V in H_2SO_4 1 M and between 1 and 7 V in H_2SO_4 0.1 M. The current densities on the "plateau" remain relatively high, around 50 mA cm^{-2}, which means that this "passivation state" does not correspond to the formation of a highly blocking conversion layer. Outside the narrow passivation ranges, the current density, corresponding to Co oxidation and dissolution into Co^{2+}, is limited by the conductivity of the electrolytic medium. Therefore, the slope increases with the electrolyte concentration.

Whatever the electrolyte concentration, the anodizing of pure Sb (Fig. 1b) leads to the formation of an insulating barrier film over the explored potential range 0–40 V, as revealed by the current densities remaining very low. This observation is in good agreement with previous studies performed in various media, over narrower potential ranges [13–16].

The anodic behavior of $CoSb_3$ is similar to this of pure Sb until 3 V (Fig. 1c) and seems to be independent of the electrolyte concentration. A first passivation state is actually observed, with very low current densities between 1 and 5 mA cm^{-2}. The electrochemical interface then undergoes a modification and obviously reaches a second passivation state beyond 8 V, less blocking than the first one as shown by the current densities more than one order of magnitude higher, between 50 and 80 mA cm^{-2}. Therefore, forming a barrier layer on $CoSb_3$ at low potential seems to be more judicious.

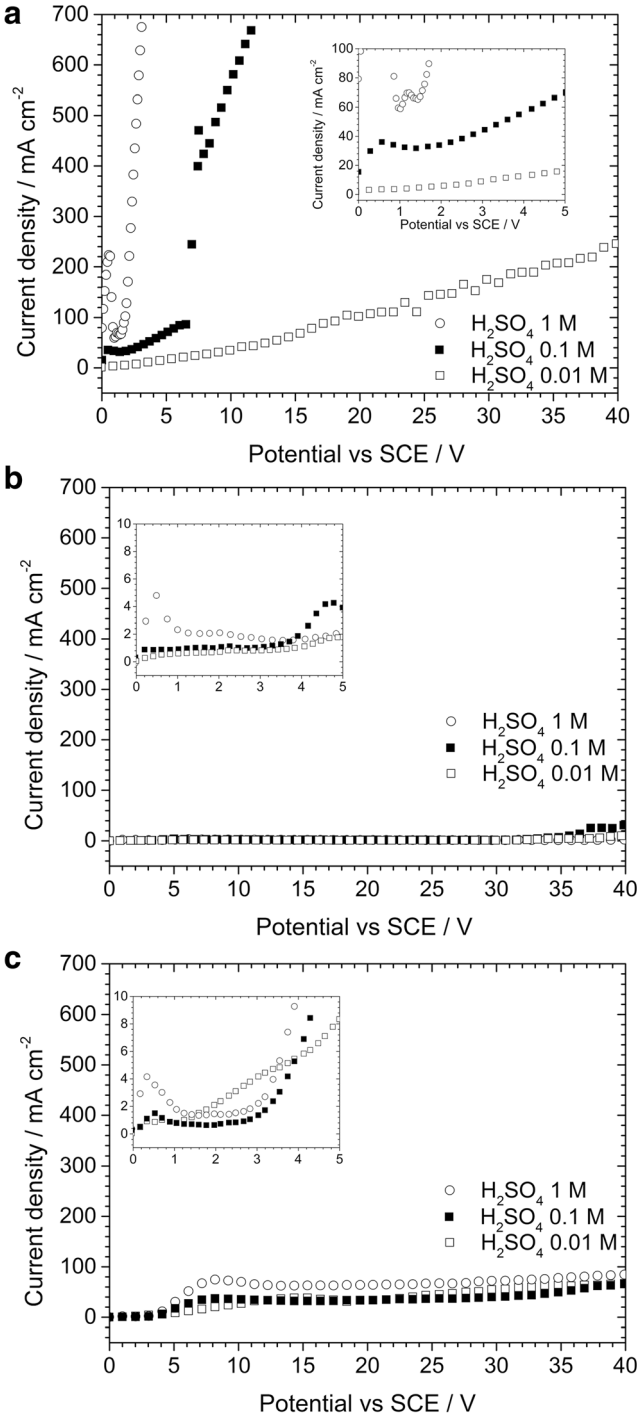

Fig. 1 Potentiodynamic polarization curves recorded at 40 mV s^{-1} in H_2SO_4 solution with different concentrations: pure Co (**a**), pure Sb (**b**), and $CoSb_3$ (**c**)

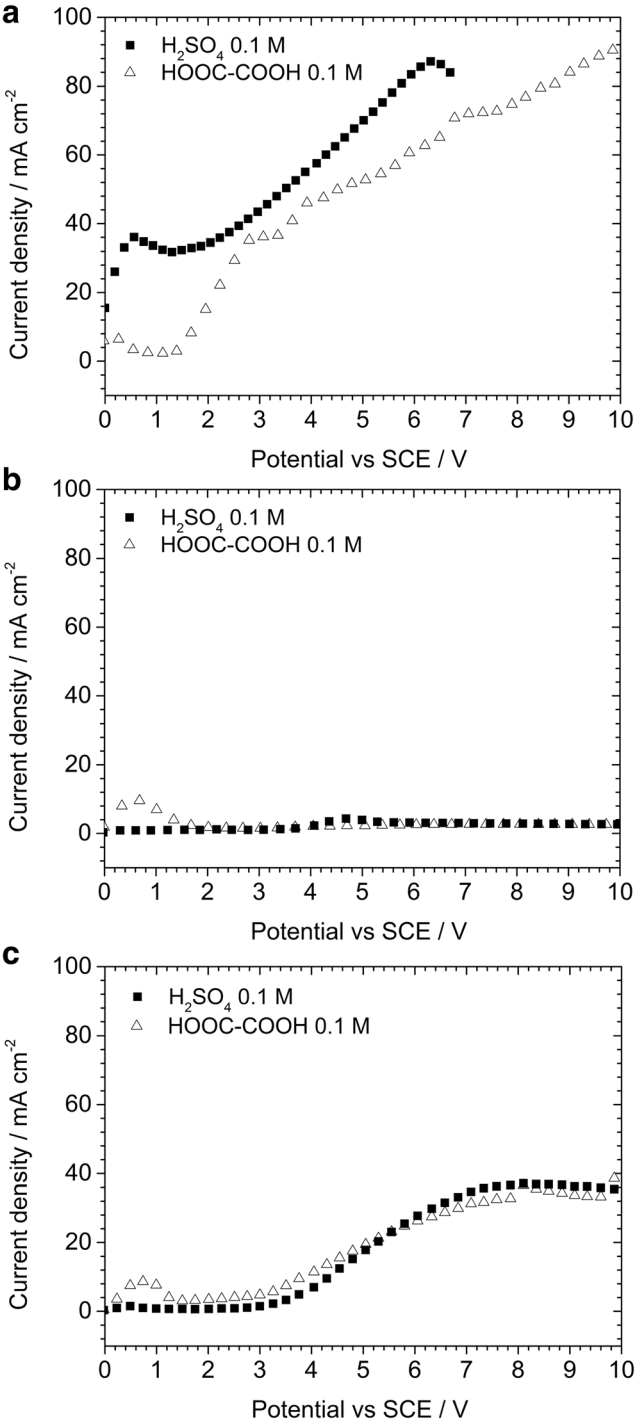

Fig. 2 Potentiodynamic polarization curves recorded at 40 mV s^{-1} in H_2SO_4 and HOOC–COOH 0.1-M solutions: pure Co (**a**), pure Sb (**b**), and $CoSb_3$ (**c**)

And since the first passivation plateau is the longest in 0.1 M H_2SO_4, this concentration appears as the most appropriate and will be taken as a reference thereafter.

In comparison with sulfuric acid, oxalic acid seems to induce little change in the anodic behavior of Co, Sb, and $CoSb_3$ (Fig. 2). Co undergoes high dissolution rate, and high current density levels are reached already at low potentials (Fig. 2a). Sb passivates with passivation current values remaining very low over the scanned potential range (Fig. 2b). $CoSb_3$ exhibits two different passivation stages (Fig. 2c), a first below 3 V and a second with higher current density values beyond 8 V. In both electrolytes, the electrochemical behavior observed on

Sb and $CoSb_3$ is similar between 0 and 3 V. Indeed, the current densities remain very low, below 10 mA cm^{-2} and, in the specific case of polarization in oxalic acid, a first oxidation "peak" between 0 and 1 V precedes the first passivation.

According to the electrochemical study related above, the potential range of interest for the formation of a highly passivating conversion layer on $CoSb_3$ is confined between 1 and 3 V whatever the considered electrolyte. Therefore, the growth of the anodic layers was performed by applying 2 V during 60 min.

The resulting chronoamperometric curves are displayed in Fig. 3. During the 6 first minutes, the current density is stable at a value of around 5 mA cm^{-2}, consistently with the passivation current measured throughout the voltamperometric study (Fig. 2c). Then, the current density slightly increases concomitantly in both electrolytes until reaching 12 mA cm^{-2} after 10 min of potentiostatic treatment. The next step in the anodizing process depends on the nature of the acid from the electrochemical point of view. Whereas the current density in oxalic acid rapidly stabilizes after a maximum at 8 mA cm^{-2}, its rising continues in sulfuric acid until 30 min of treatment. During the last 30 min of anodic oxidation, the current density remains quasi-constant between 32 and 37 mA cm^{-2}, namely in the magnitude order of the value measured on the "second passivation plateau" observed beyond 7 V throughout the voltamperometric study (Fig. 2c).

Morphology and composition of the conversion layers

The morphology of the conversion layers grown by potentiostatic anodic polarization (2 V, 60 min) in sulfuric acid or oxalic acid is shown in Figs. 4 and 5, respectively. In both cases, conversion products obviously cover the $CoSb_3$ metallic substrate (Figs. 4a, b and 5a, b). According to cross-sectional micrographs (Figs. 4c and 5c), the layer grown in sulfuric acid is about 20 μm thick, and the one grown in oxalic acid is 40 μm thick. In both cases, the inside of the layer appears highly porous. More precisely, as evidenced by high magnification images (Figs. 4d and 5d), numerous cracks are homogenously dispersed within the layer, lying parallel to the substrate surface. This results in a laminated aspect of the coating inside (Figs. 4c and 5c) and a powdered aspect of the conversion products on surface (Figs. 4a, b and 5a).

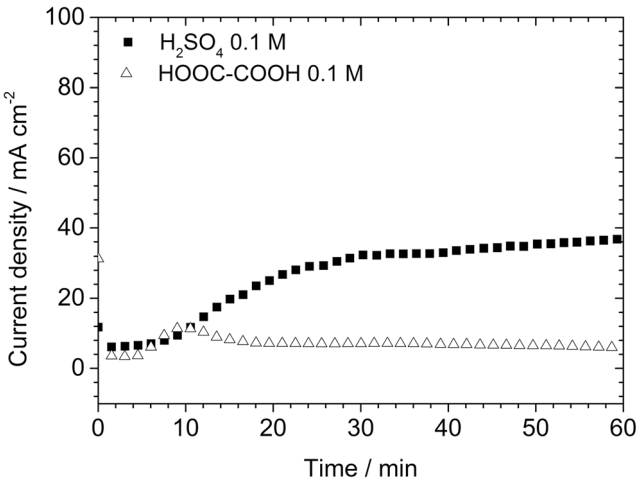

Fig. 3 Chronoamperometric curves recorded during polarization of $CoSb_3$ at 2 V in H_2SO_4 and HOOC–COOH 0.1-M solutions

Regarding the composition of the conversion products formed in sulfuric acid, EDS analyses performed on the cross section (Fig. 4c) reveal the presence of Sb and O and a small amount of S, but no Co could be detected. However, according to XRD pattern (Fig. 6), no supplementary crystallized phase could be identified in comparison with untreated $CoSb_3$ substrate. Consequently, the conversion products likely consist of amorphous antimony oxides on which sulfates adsorb.

In the specific case of anodizing in oxalic acid, besides the porous-exfoliated "matrix" (Fig. 5c), nanosized rods can be distinguished on the extreme surface (Fig. 5b) and in the interfoliar spaces of the cracked layer (Fig. 5d). Unlike the homogeneous contrast observed on the anodic layer grown in sulfuric acid (Fig. 4c), the porous network formed in oxalic acid seems to exhibit different chemical properties (composition, hydration level) or different physical properties (density). Actually, according to EDS analysis (Fig. 7), only Sb and O elements could be identified whatever the considered area of the "matrix," with obviously a less amount of Sb in the upper part of the antimony oxide layer. The corresponding antimony oxide remains mainly not or poorly crystallized and therefore are not detected in the relative diffraction pattern (Fig. 6).

Nevertheless, a crystalline phase could be identified in this diffraction pattern as $Sb(C_2O_4)(OH)$ [21]. This phase could correspond to the nanosized rods. Indeed, by EDS analysis of the areas rich in tangled sticks and in the outermost part of the conversion layer, relative high level of O and C, associated with Sb (lower content than in the oxide "matrix") could be evaluated. Co was also detected in these specific areas, indicating a probable presence of cobalt oxalate or cobalt hydroxy-oxalate.

Discussion

In the present work, the electrochemical conversion of $CoSb_3$ intermetallic phase has been investigated in acidic media in comparison with pure Co and Sb. The electrochemical study, carried out over a wide potential range (0–40 V), has shown that the behavior of the considered intermetallic phase $CoSb_3$ is close to the one of pure Sb, with current densities remaining low regarding the values reached during the oxidation of pure Co. Actually, outside a restricted potential range, Co undergoes oxidation into Co^{2+} with a the dissolution rate limited by the conductivity of the medium. On the "pseudo

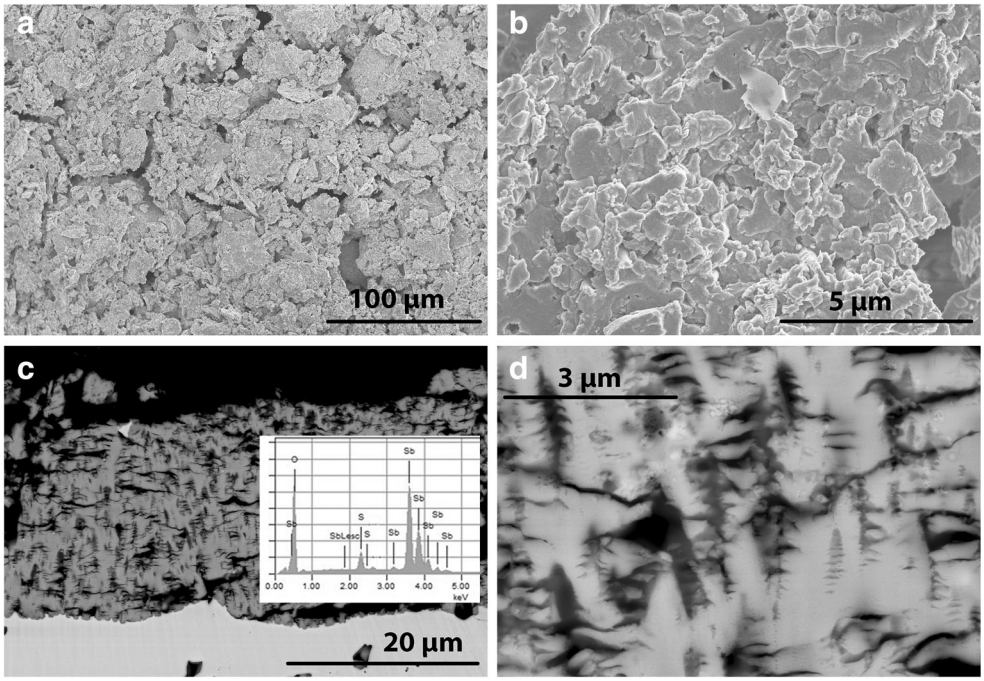

Fig. 4 Surface (**a**)(**b**) and cross-sectional (**c**)(**d**) SEM observations of conversion layers grown by anodic polarization (2 V, 60 min) of $CoSb_3$ in H_2SO_4 0.1 M

passivation plateau," even in optimal acidic concentration conditions (0.1 M, giving the longest plateau (0–7 V)), the current density is one order of magnitude higher on Co than on Sb or $CoSb_3$.

Consequently, as confirmed by EDS analysis, the potentiostatic anodizing of $CoSb_3$ at 2 V results in the formation of an amorphous oxide layer containing only Sb due to the selective dissolution of Co on the one hand and selective anodizing of Sb on the other hand. This phenomenon corresponds to a dealloying of the starting $CoSb_3$ intermetallic phase. Numerous examples of dealloying can be found in the recent literature, leading most of the time to the formation of a nanostructured metallic network [22–24], as a consequence of the selective dissolution of one element. But few references deal with the formation of simple oxide on alloys by dealloying under the effect of anodic polarization [25, 26].

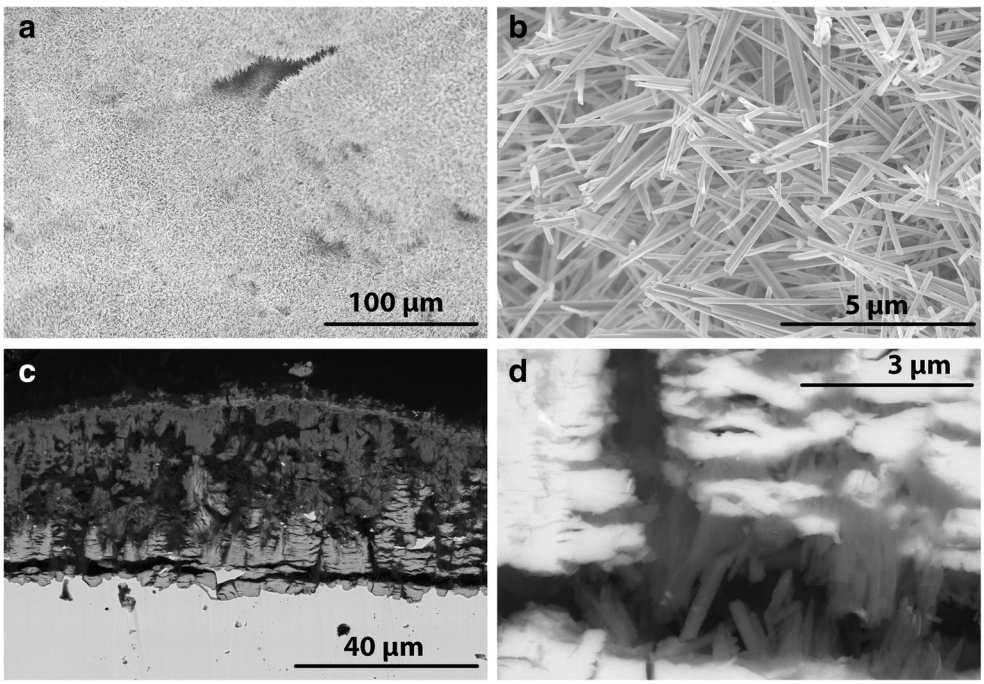

Fig. 5 Surface (**a**)(**b**) and cross-sectional (**c**)(**d**) SEM observations of conversion layers grown by anodic polarization (2 V, 60 min) of $CoSb_3$ in HOOC–COOH 0.1 M

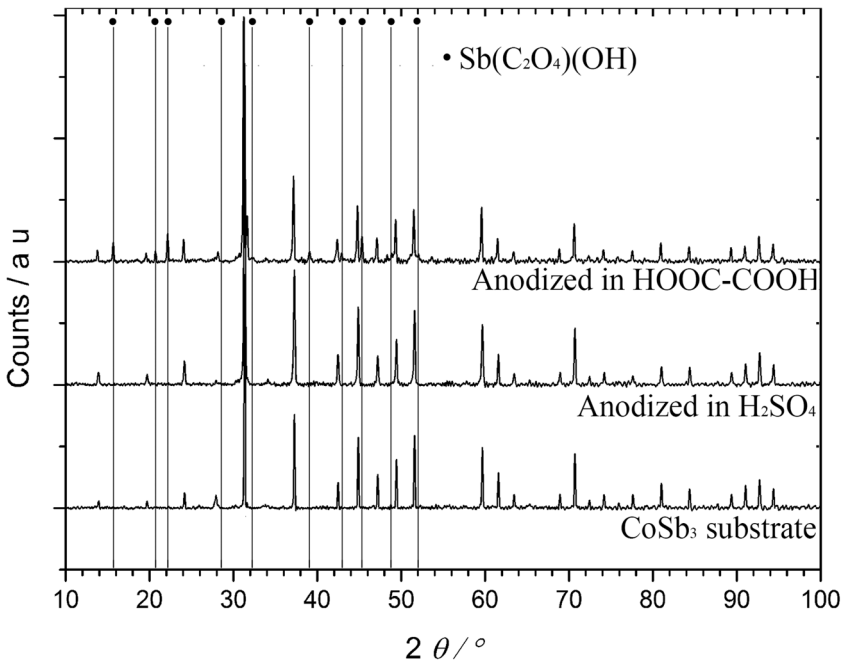

Fig. 6 XRD patterns of $CoSb_3$ substrate and $CoSb_3$ anodically polarized (2 V, 60 min) in H_2SO_4 and HOOC–COOH 0.1 M, respectively

In the present case, the antimony oxide "matrix" resulting from the anodizing of $CoSb_3$ intermetallic phase is as expected highly porous, as shown by SEM images. According to the potentiodynamic studies, the electrochemical behavior of $CoSb_3$ differs from the one of pure Sb beyond 4 V whatever the electrolyte and its concentration.

Actually, due to the undergone dealloying, the anodized layer grown on $CoSb_3$ suffers from a lack of material regarding the one grown on pure Sb, and a local atomic rearrangement is necessary. The induced local mechanical stress may be accommodated until a critical thickness. Then, the oxide layer cracks. This critical thickness seems to mark the starting point of a second anodizing stage, characterized by a higher (one order of magnitude) but constant current density.

On this second "passivation plateau," the main part of the current can be likely assigned to water oxidation (in competition with the oxide formation), whose rate is limited by the diffusion of the generated oxygen through the conversion

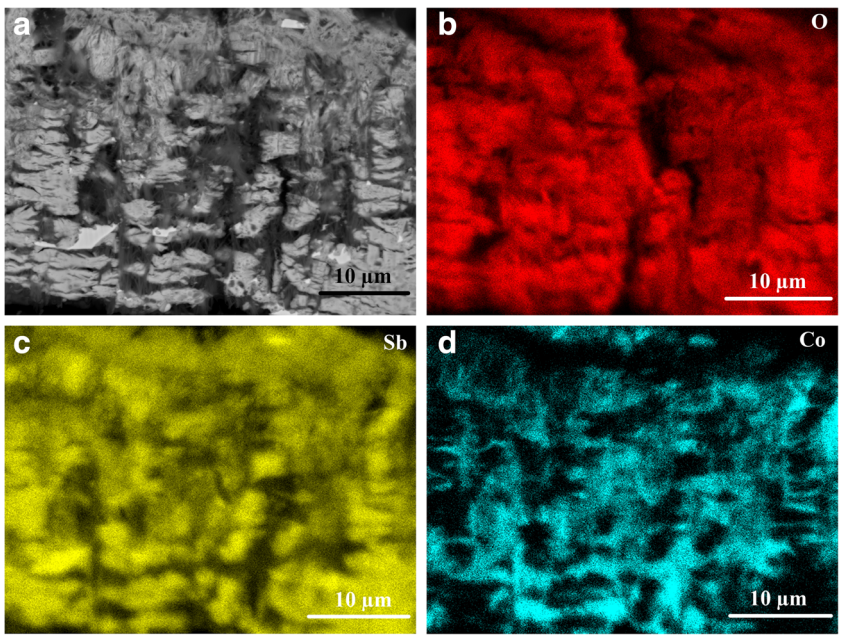

Fig. 7 Cross-sectional analysis of a conversion layer grown by anodic polarization (2 V, 60 min) of $CoSb_3$ in HOOC–COOH 0.1 M: BSE (**a**), EDS maps of O (**b**), Sb (**c**), and Co (**d**)

layer. Moreover, oxygen bubbling can contribute to the porosity of the oxide network.

In the conditions of potentiostatic oxidation of $CoSb_3$ in sulfuric acid at 2 V, the critical conditions of the film breakdown seems to be reached after 6 min of anodic polarization. Then, the anodizing regime seems to be similar to the "high potential" anodizing regime of $CoSb_3$, according to the very similar current density values.

In the specific conditions of anodizing performed in oxalic acid, the cracking of the oxide matrix obviously occurs at the same time as in sulfuric acid. Similarly, the current density starts increasing, as a consequence of water oxidation enhancement and metallic dissolution acceleration. Due to metallic ions accumulation in the confined areas, the solubility constants of oxalate hydroxides are exceeded. Oxalate hydroxides precipitate in the porosities within the oxide layer and on the surface, as observed on SEM images. Indeed, the corresponding rods have been identified by combining EDS and XRD analyses.

These entangled rods therefore fill the porosities of the oxide matrix, limiting the diffusion of oxygen through the oxide layer, and as a consequence the water oxidation rate. In sulfuric acid, the current density increase after the mechanical breakdown of the oxide layer is precisely due to the increase of the water oxidation, in competition with the anodic layer formation. The precipitation of oxalate prevents from this water oxidation intensification, and the current density remains therefore low during the potentiostatic polarization. Moreover, the antimony oxide matrix is protected from alkaline dissolution, and the anodized layer grown in oxalic acid is thicker than the one grown in sulfuric acid.

Finally, according to the chemical nature of the anodic layers grown (simple antimony oxide) and their high level of porosity, they cannot be considered as potential protective barrier against high temperature oxidation.

Conclusions

Electrochemical conversion layers were formed and investigated for the first time on $CoSb_3$ thermoelectric material. Chemical and electrochemical parameters directly influence the growth and the properties of the passivating layer. In sulfuric and oxalic acid, the dealloying of $CoSb_3$ intermetallic phase induces the growth of a porous and amorphous simple antimony oxide. In presence of oxalic acid, nanosized sticks of metallic oxalate hydroxides precipitate within the cracks and on the surface of the antimony oxide network.

Acknowledgements The French National Research Agency (ANR) is gratefully acknowledged for financial support of the post-doctoral position of Richard Drevet in the project Nanoskut (ANR-12-PRGE-0008-01).

References

1. Kawaharada Y, Kurosaki K, Uno M, Yamanaka S (2001) Thermoelectric properties of $CoSb_3$. J Alloy Compd 315(1-2):193–197
2. Hara R, Inoue S, Kaibe HT, Sano S (2003) Aging effects of large-size n-type $CoSb_3$ prepared by spark plasma sintering. J Alloy Compd 349(1-2):297–301
3. Godlewska E, Zawadzka K, Adamczyk A, Mitoraj M, Mars K (2010) Degradation of $CoSb_3$ in air at elevated temperatures. Oxid Met 74(3-4):113–124
4. Leszczynski J, Wojciechowski KT, Malecki AL (2011) Studies on thermal decomposition and oxidation of $CoSb_3$. J Therm Anal Calorim 105(1):211–222
5. Zhao D, Tian C, Liu Y, Zhan C, Chen L (2011) High temperature sublimation behavior of antimony in $CoSb_3$ thermoelectric material during thermal duration test. J Alloy Compd 509(6):3166–3171
6. Godlewska E, Zawadzka K, Mars K, Mania R, Wojciechowski K, Opoka A (2010) Protective properties of magnetron-sputtered Cr-Si layers on $CoSb_3$. Oxid Met 74(3-4):205–213
7. Zhao D, Zuo M, Wang Z, Teng X, Geng H (2014) Protective properties of magnetron-sputtered Ti coating on $CoSb_3$ thermoelectric material. Appl Surf Sci 305:86–92
8. Xia X, Huang X, Li X, Gu M, Qiu P, Liao J, Tang Y, Bai S, Chen L (2014) Preparation and structural evolution of Mo/SiOx protective coating on $CoSb_3$-based filled skutterudite thermoelectric material. J Alloy Compd 604:94–99
9. Zhao D, Zuo M, Teng X, Geng H (2014) Thermal aging behavior of $CoSb_3$ with protective Mo coating. Mater Sci Forum 787:215–220
10. Zhao D, Bai S, Ma Q, Zuo M, Teng X (2015) Protective properties of YSZ/Ti film deposited on $CoSb_3$ thermoelectric material. Corros Sci 98:163–169
11. Zhao D, Wu D, Niang J, Zuo M (2017) Protective properties of various coatings of $CoSb_3$ thermoelectric material. J Electron Mater 46(5):3036–3042
12. Zawadzka K, Godlewska E, Mars K, Nocun M, Kryshtal A, Czyrska-Filemonowicz A (2017) Enhancement of oxidation resistance of $CoSb_3$ thermoelectric material by glass coating. Mater Design 119:65–75
13. Pavlov D, Bojinov M, Laitinen T, Sundholm G (1991) Electrochemical behaviour of the antimony electrode in sulphuric acid solutions—II formation and properties of the primary anodic layer. Electrochim Acta 36(14):2087–2092
14. Bojinov M, Kanazirski I, Girginov A (1995) Anodic film growth on antimony in H_3PO_4 solutions. Electrochim Acta 40(7):873–878
15. Mogoda AS, Abd El-Haleem TM (2003) Anodic oxide formation on antimony and its currentless dissolution in sulphuric acid containing some monocarboxylic acids. Thin Solid Films 441(1-2):6–12
16. Linarez Perez OE, Perez MA, Teijelo ML (2009) Characterization of the anodic growth and dissolution of antimony oxide films. J Electroanal Chem 632(1-2):64–71
17. Konno Y, Tsuji E, Skeldon P, Thompson GE, Habazaki H (2012) Factors influencing the growth behavior of nanoporous anodic films on iron under galvanostatic anodizing. J Solid State Electrochem 16(12):3887–3896
18. Gui Q, Yu D, Zhang S, Xiao H, Yang C, Song Y, Zhu X (2014) Influence of anodizing voltage mode on the nanostructure of TiO_2 nanotubes. J Solid State Electrochem 18(1):141–148
19. Veys-Renaux D, Rocca E (2015) Initial stages of multi-phased aluminium alloys anodizing by MAO: micro-arc conditions and electrochemical behavior. J Solid State Electrochem 19(10):3121–3129
20. Veys-Renaux D, Chahboun N, Rocca E (2016) Anodizing of multiphase aluminium alloys in sulfuric acid: in-situ electrochemical behaviour and oxide properties. Electrochim Acta 211:1056–1065
21. Kaduk JA, Toft MA, Golab JT (2010) Crystal structure of antimony oxalate hydroxide $Sb(C_2O_4)OH$. Powder Diffract 25(01):19–24

22. Hakamada M, Mabuchi M (2009) Fabrication of nanoporous palladium by dealloying and its thermal coarsening. J Alloy Compd 479(1-2):326–329
23. Gan YL, Yang Y, Du JJ, Zhang RH, Dai ZX, Zhou XW (2015) Studies on the synthesis, dealloying, and electrocatalytic properties of CoPd nanocatalysts. J Solid State Electrochem 19(6):1799–1805
24. Choi WS, Chang W, Shin HS (2014) Hollow nanodendritic nickel oxide networks prepared by dealloying of nickel-copper alloys. J Solid State Electrochem 18(2):427–433
25. Zhu SL, He JL, Zhang XJ, Cui ZD, Pi LL (2011) Ti oxide nanoporous surface structure prepared by dealloying of Ti-Cu amorphous alloy. Electrochem Commun 13(3):250–253
26. Li G, Zhang X, Song X, Sun Z, Feng W (2015) Preparation of nanoporous Ag@TiO_2 ribbons through dealloying and their electrocatalytic properties. J Solid State Electrochem 19(4):967–974